

Facet-Selective Nucleation and Conformal Epitaxy of Ge Shells on Si Nanowires

Binh-Minh Nguyen,^{*,†,‡} Brian Swartzentruber,[§] Yun Goo Ro,[‡] and Shadi A. Dayeh^{*,†,‡,||}

[†]Center for Integrated Nanotechnologies, Los Alamos National Laboratory, Los Alamos, New Mexico 87545, United States

[‡]Department of Electrical and Computer Engineering, University of California San Diego, La Jolla, California 92093, United States

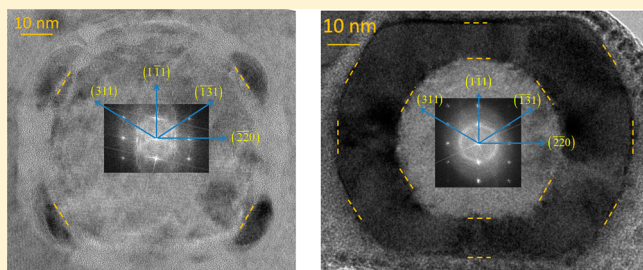
[§]Center for Integrated Nanotechnologies, Sandia National Laboratories, Albuquerque, New Mexico 87185, United States

^{||}Materials Science Program, University of California San Diego, La Jolla, California 92093, United States

Supporting Information

ABSTRACT: Knowledge of nanoscale heteroepitaxy is continually evolving as advances in material synthesis reveal new mechanisms that have not been theoretically predicted and are different than what is known about planar structures. In addition to a wide range of potential applications, core/shell nanowire structures offer a useful template to investigate heteroepitaxy at the atomistic scale. We show that the growth of a Ge shell on a Si core can be tuned from the theoretically predicted island growth mode to a conformal, crystalline, and smooth shell by careful adjustment of growth parameters in a narrow growth window that has not been explored before. In the latter growth mode, Ge adatoms preferentially nucleate islands on the {113} facets of the Si core, which outgrow over the {220} facets. Islands on the low-energy {111} facets appear to have a nucleation delay compared to the {113} islands; however, they eventually coalesce to form a crystalline conformal shell. Synthesis of epitaxial and conformal Si/Ge/Si core/multishell structures enables us to fabricate unique cylindrical ring nanowire field-effect transistors, which we demonstrate to have steeper on/off characteristics than conventional core/shell nanowire transistors.

KEYWORDS: Si, Ge, core/shell, nanowire, nucleation, facet, misfit dislocation, FET



Heterostructured semiconductor core/shell nanowires¹ (NWs) are highly desirable for advanced electronic and optoelectronic devices; however, realizing core/shell or core/multishell NW structures is often quite challenging due to different growth conditions of the dissimilar materials. Along with the challenges found in heterostructured thin films, growing core/shell NWs has additional complexity due to new emerging phenomena in nanoscale epitaxy.^{2–7} On the other hand, heterostructured core/shell NWs possess the advantage of a larger critical thickness due to core/shell strain sharing.⁸ For the Si/Ge material system, Ge-core/Si-shell structures are quite advanced in both material development^{1,5,8–11} and device applications.^{12–23} Conversely, a functional device fabricated from a Si-core/Ge-shell counterpart has yet to be shown, despite a lot of theoretical interest.^{24–30} The technical challenge in growing high quality, conformal Ge shells on Si NWs has long impeded the realization of Si/Ge core/shell NW devices. Although the first report of core/shell NWs demonstrated both Ge/Si and Si/Ge core/shell structures,¹ later experiments by Pan et al.³¹ revealed a dominant Stranski–Krastanov growth mode of Ge on Si NW cores, where Ge islands form after the growth of a thin wetting layer. Independent theoretical work^{4,10} reconciled the two observations by a size-dependent interplay between the mismatch strain and the surface energy, suggesting a conformal shell growth mode for NWs with diameters less

than 15 nm and island formation on larger diameter NWs. Although this prediction was experimentally validated,³² several groups reported conformal coverage of Ge shells on a broad range of Si NW diameters,^{33–36} but an in-depth analysis of the crystal structure and morphology evolution of the deposited shells has yet to be developed. It is important to emphasize that the theoretical models^{4,10} treated the core/shell NWs as a simple isotropic elastic media with no well-defined crystallographic faceting. However, it has been shown that facets on the Si NWs play an important role in the nucleation of Ge.^{31,36} Recently, Kempa et al. demonstrated different growth modes of Ge on Si NWs by varying growth conditions (precursor gases).³⁶ Here, we show that such growth-mode transitions can be obtained under the same reactor gas flow conditions. More precisely, we observed island-like Ge growth at high growth temperatures, whereas at lower temperatures, we found conformal epitaxy of the Ge shells. Such conformal deposition did not start isotropically, but rather with nucleation of islands on {113} facets and then on {111} facets. As the growth proceeded, the islands coalesced into a conformal shell at directionally different growth rates. We hypothesize that strain

Received: June 11, 2015

Revised: September 24, 2015

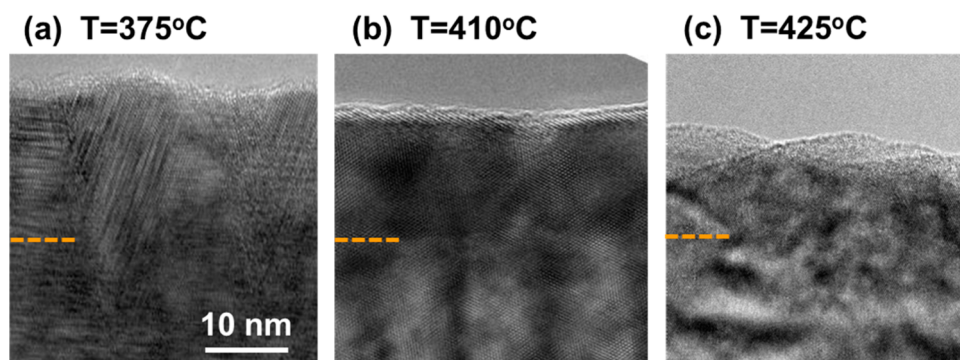


Figure 1. Transmission electron microscopy of Si/Ge core/shell NWs grown at (a) 375 °C, (b) 410 °C, and (c) 425 °C. Growth times were adjusted in order to achieve similar shell thicknesses for all three samples. All panels share the same scale bar.

relaxation through misfit dislocations at the island growth stage allows for the possibility of perfect coalescence with defect-free coalescence boundaries. With the high crystalline quality of deposited thin Ge shells on Si nanowires, we demonstrated the first prototype of cylindrical ring channel NWFETs with steeper subthreshold characteristics than reference Ge-core/Si-shell NWFETs.

The Si/Ge core/shell NWs in this work were grown on Si (111) substrates in a low pressure, cold wall chemical vapor deposition (CVD) system. The Si cores were grown at 460 °C using 450 sccm SiH₄ (50% diluted in H₂) at 0.5 Torr pressure from Au colloid seeds with nominal diameters of 10, 40, and 80 nm. Under such conditions, most Si NWs grew along $\langle 112 \rangle$ directions. The substrates were then cooled down to the Ge shell deposition temperature without any stabilizing gas. The growth conditions for Ge shell were optimized by tuning growth temperature and pressure. Shown in Figure 1 are transmission electron microscopy (TEM) images of typical NW morphology grown at 375, 410, and 425 °C. Growth time was adjusted to obtain more or less the same shell thickness at all temperatures. At low temperatures (375 °C and below), conformal Ge shells were deposited, but with poor crystallinity. This is likely due to the low mobility of Ge adatoms at low temperature, only allowing them to position where they are adsorbed; the shells are thus conformal but defective. At a slightly higher temperature (~ 410 °C), the adatoms gain enough mobility to diffuse and rearrange to enhance local crystallinity, resulting in smoother and still conformal shells. At higher temperatures (above 425 °C), the Ge adatoms can diffuse even more freely and tend to bind with other Ge atoms rather than with Si atoms; hence, the formation of islands similar to previous observations.^{31,32} Although theory predicts a more energetically favorable configuration of 3D islands over conformal 2D shells for Si/Ge core/shell nanowires,^{4,6,10,37} the contradicting experimental evidence presented in this work and in refs 1 and 33–36 suggests that a pure static stress model is not adequate. Compared with previous works,^{1,30–33} our fine growth condition at around 410 °C possesses higher crystal quality and unprecedentedly discussed nucleation stage, as will be detailed below. Although the growth temperature had a strong effect on the NW morphology, the GeH₄ (30% in H₂) partial pressure in the range of 5 mTorr to 150 mTorr (corresponding to chamber pressure of 100 mTorr to 500 mTorr) does not appear to affect the shell morphology (conformal shell vs island) but rather only the deposition rate. We obtained the most controllable and reproducible shell growth with a slow growth rate (~ 0.5 nm/min) using 50 sccm

GeH₄ further diluted in 200 sccm H₂ with no regulated pressure (baffle valve fully open). The corresponding GeH₄ partial pressure and chamber pressure were 5 mTorr and 100 mTorr, respectively. As will be shown later and in Supporting Information, the facet-selective nucleation and growth of the Ge shell hinders any deeper assessment of the growth rate.

To understand the Ge shell growth mechanism on Si nanowires, we performed ex-situ studies of the evolution of the shell morphology at different growth times/stages using the optimal shell growth temperature of 410 °C, which rendered conformal, crystalline shells (Figure 1b). NWs with different core diameters exhibited the same trend (see Supporting Information Figure S1) but the quality of the core Si NWs appears to be better with larger Si diameter, so we focus on results from NWs mediated from 80 nm Au colloids in this report. Figure 2 shows side view SEM and cross sectional TEM micrographs of 80 nm diameter Si-core NWs with 15, 30, and 60 min of Ge shell deposition and a schematic illustration for the observed growth evolution on the Si nanowire facets. As can be seen in the SEM image set, Ge shell growth starts by forming isolated islands that grow bigger and coalesce into a conformal, smooth shell. Although the side view TEM micrographs of the Ge islands (see Supporting Information) look similar to published results in the literature,^{31,32} it is clear in lower magnification SEM images (Figure 2a) that the Ge islands do not form isotropically on the core surface like theories suggested,^{4,6,10,37} but rather align along particular ridges. More strikingly, despite initial roughness, the Ge shell can quickly grow into a smooth, conformal shell at a shell thickness as thin as 15 nm, with no sign of degradation with thickness (up to 50 nm shells were tested).

Island formation along ridges and faceted shell deposition indicate the incorporation of Ge is anisotropic. In order to achieve a better insight on this phenomenon, NWs were cut perpendicular to the growth direction into ~ 100 nm thick slices using focused ion beam (FIB) for cross sectional TEM imaging. Figure 2d shows the cross-sectional TEM image of a Si/Ge NW with 15 min shell deposition. Fast Fourier transforms of lattice-resolved images confirm the growth direction (parallel to beam axis) to be $\langle 112 \rangle$. Ge islands nucleated on the four $\{113\}$ corner facets. Direct measurement of the lattice spacing from HRTEM images (see Supporting Information Figure S2) yields (111) lattice spacings of (mostly) relaxed Ge islands ($a_{(111)} = 3.24$ Å) on the Si core ($a_{(111)} = 3.15$ Å). This relaxation is also confirmed by the Moiré fringes in side view TEM images of NWs with thick Ge shells (see Supporting Information Figure S3), as a result of the superposition between the Ge and Si

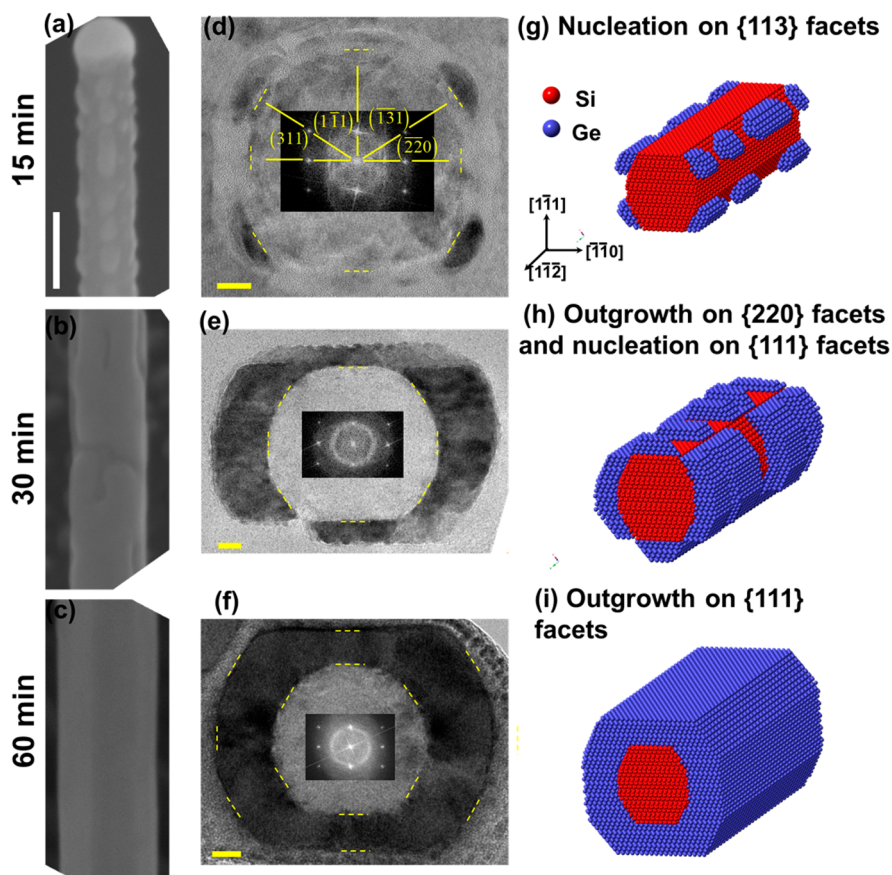


Figure 2. (a)–(c) Side view SEM, (d)–(f) cross-sectional TEM, and (g)–(i) schematic cartoons illustrating the growth process (right column) of 80 nm diameter Si-core (bright contrast)/Ge-shell (darker contrast) NWs as a function of growth time. In panels d and e, the bright contrast region outside the NW is an Al_2O_3 dielectric layer to protect the NWs from FIB damage and enhance Ge shell boundary contrast. In panel f, the outer dark contrast is the protective Pt layer. The scale bar for all SEM images is 100 nm, and the scale bar for all TEM images is 10 nm. A clear transition from faceted island nucleation (15 min growth time) to faceted conformal shells (60 min growth time) was observed.

lattices. From the Moiré periodicity, we estimate a lattice mismatch of 4–5%, which is very close to the relaxed lattice mismatch of 4.2% between Ge and Si.

The cross-sectional TEM images of 30 and 60 min NW shell growth are shown in Figure 2e,f. At 30 min (Figure 2e), the Ge regions with darker contrast are in focus, whereas the lighter regions (top (111) plane and right corner of the bottom (111) plane) are defocused, indicating they belong to other islands that might have grown earlier/faster and have already merged into the conformal shell. For the view plane that is in focus (dark contrast), the {113} Ge islands already coalesced over the {220} facets, whereas they remained disconnected across the {111} facets. The bottom (111) facet developed an island on its own that expanded laterally to merge with growing {113} islands on both sides. At 60 min (Figure 2f), the Ge shell was fully merged and conformally covered the core. Although in situ cross sectional monitoring of the shell evolution is not possible, the Ge morphologies shown here are typical for each growth time (see Supporting Information for additional cross sectional TEMs), thus enabling us to predict the growth evolution as illustrated in the schematic cartoon in Figure 2g.

Facet selective growths on Si NWs has been reported for Ge³⁶ and compound semiconductor shell;³⁸ however, there are clear distinction between this work and previous results. The previous facet selective growths were reported to be a completely different growth mode than conformal shell conditions, and required a different gas-phase species³⁶ or the

presence of a thin oxide film on a particular facet family.³⁸ In this work, we studied the temporal evolution of the shell growth and showed that the facet selective nucleation was an early stage of the conformal shell epitaxy under the same conditions. As more materials were deposited, the isolated nucleation islands grew both along the growth direction and around the circumference to coalescence into smooth, conformal shell. The contrast between our facet-selective isolated islands and the continuous strips of shell along specific facets is topologically analogous to the difference between the Plateau–Rayleigh crystal growth mode³⁹ and the continuous shell even though the competition between adatom diffusion and surface bonding energy could be at different level. In addition to the static stress models for core/shell stability,^{4,6,10,37} recent observations in refs 36, 38, and 39 and in this work clearly evidenced the kinetic role of adatoms diffusions; therefore, a theoretical model to combine the two mechanisms is highly desirable to explain the diverse appearance of heterogeneous core/shell growths.

It is important to note that the transition from islands to a conformal Ge shell is in contrast with the case of Ge-core/Si-shell NWs where a thin Si shell (1 to 3 nm) can be conformally deposited on the Ge core before roughening at larger shell thicknesses.^{5,8} This difference between Ge on Si vs Si on Ge is similar to the trend in planar growth and is attributed to the sign of the strain: tensile $\text{Si}_{0.5}\text{Ge}_{0.5}$ grown on Ge substrates tends to be smoother than compressive $\text{Si}_{0.5}\text{Ge}_{0.5}$ films on Si

substrates, which is more prone to surface undulations.⁴⁰ However, there might be other possible explanations. For example, the surface tension between Si and Ge might be such that Si “wets” Ge, making it energetically favorable for a Si atom to bond directly to a Ge atom on the Ge NW core, whereas Ge does not wet Si and prefers to bond with other Ge shell atoms rather than Si atoms on the Si core.

Despite the lack of an in situ characterization technique to observe the island evolution during growth, we can still trace the coalescence by comparing different pairs of islands in 30 min shell growths on Si NWs. In Figure 3b, two islands have

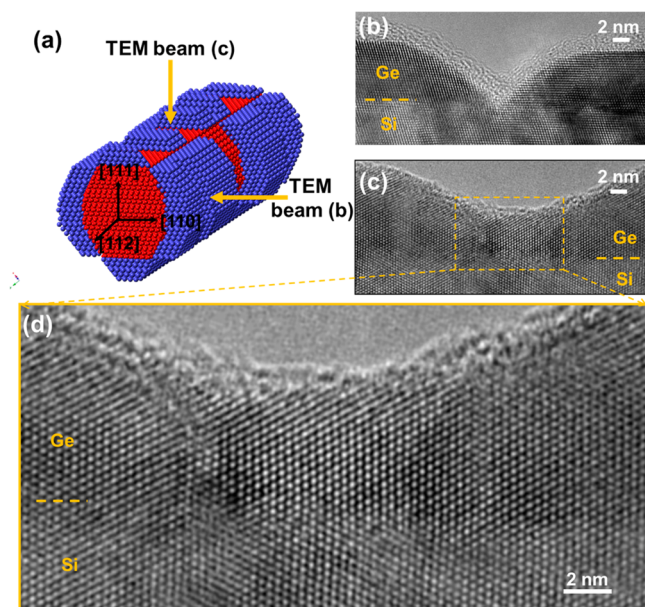


Figure 3. (a) Cartoon illustration of TEM beams with respect to the NW orientation, HRTEM of Ge islands on Si core after 30 min shell growth. (b) Sample A: 2 islands start to coalesce. (c) Sample B: coalescence already took place. (d) Zoomed-in view of the box in (c), indicating high crystallinity of merged region with no dislocations.

grown both horizontally (axially) and vertically (radially) to the point that they start to merge. The (111) lattice spacings are measured to be $a_{(111)} = 3.23 \text{ \AA}$ for the Ge shell, $a_{(111)} = 3.12 \text{ \AA}$ for the Si core, indicating again that the Ge islands are already mostly relaxed. Misfit dislocations (one missing lattice plane in Ge compared to in Si) are observed in the island, but there is no correlation with the merging of the islands. For example, in Figure 3c and d, a coalesced area was viewed in high-resolution mode, showing no sign of dislocations or defects.

The fact that the Ge islands nucleate first on the {113} facets is neither predicted by theory nor previously observed for Ge/Si NWs. However, it is not unprecedented. Despite {111} facets having the lowest surface energy,⁴¹ it has been shown that {113} facets are favorable over {111} facets for selectively grown Si on patterned Si (100) surfaces due to growth kinetics rather than surface energy differences.⁴¹ This is supported in our experiments by the fact that the transition between island vs smooth shell growth modes occurs at different temperatures while every other parameter remained the same, indicating that the growth of Ge on Si core is kinetically limited. The influence of strain at the heterointerface could also be responsible. From the $\langle 112 \rangle$ beam axis, dislocations with $(a/2)\langle 110 \rangle$ Burgers have a projection of $(a/2)\langle 110 \rangle \cos(60^\circ) \cos(60^\circ) = 0.1 \text{ nm}$ in the $\langle 110 \rangle$ direction on a {112} plane, and a projection of $(a/$

$2)\langle 110 \rangle \cos(60^\circ) \cos(30^\circ) = 0.173 \text{ nm}$ in the $\langle 111 \rangle$ direction on a {112} plane. The linear density of dislocations will then be 2.5 nm in the $\langle 110 \rangle$ direction and 4.3 nm in the $\langle 111 \rangle$ direction, indicating a larger density of dislocations in the $\langle 110 \rangle$ direction at the {111} interface. This agrees qualitatively with the experimentally observed larger number of dislocations and smaller spacing on the $(\bar{1}\bar{1}1)$ plane compared to those on the $(\bar{2}\bar{2}0)$ plane (Figure 4). In other words, there is a greater strain

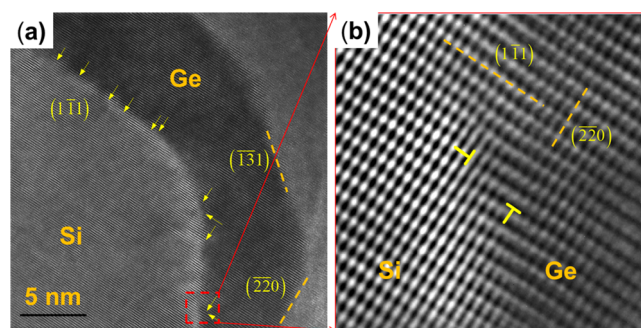


Figure 4. (a) High resolution cross sectional view of a Si-core/Ge-shell NW showing misfit dislocations in $(\bar{1}\bar{1}1)$ and $(\bar{2}\bar{2}0)$ planes. (b) FFT enhanced digital zoom-in of the area enclosed by dashed square in (a).

energy to accommodate at the {111} interface compared to the {110} interface, and as a result, the nucleation energy is higher on the former, {111}, compared to the latter, {110}, or to the superposition of the two, that is, {113} facets. This strain energy could favor nucleation of Ge islands on non-{111} facets, such as the {113} facet as we observed experimentally. The nucleation on (111) is not prohibited but is just delayed, as one can see in Figure 3h. When the growth time is long enough, in a number of NWs, the Ge shell on the (111) facets can evolve to become thicker than other facets (see Supporting Information, Figure S7).

The successful growth of conformal Ge shells on Si cores enabled us to implement a new design of a nanowire transistor: cylindrical ring channel NWFET. Our previous investigations have shown that for Ge/Si core/shell NWFETs, the subthreshold swing increases with NW diameter due to the increase of the material volume needing to be depleted.²⁰ Although larger diameter NWs enable larger transconductance,²⁰ the degradation of subthreshold swing is highly undesirable and is a limitation of NWFETs in comparison with conventional planar transistor architectures such as ultrathin body FETs (Figure 5a). In ultrathin body FETs, the subthreshold swing is dictated by the channel thickness, whereas the transconductance is governed by the transistor's width, making it possible to independently control subthreshold swing and transconductance.^{42,43} In NWFETs (Figure 5b), both figures of merit are coupled to the NW diameter, the unique degree of freedom, in opposite trends. Here, we propose a new cylindrical ring channel NW geometry that possesses an additional degree of freedom for device optimization. Instead of the solid Ge core in a Ge/Si core/shell structure, we utilize a Si core with a thin Ge shell, which has a cross-sectional cut of a ring-shape, as the conducting channel. A thin Si outer shell is added to provide carrier confinement in the Ge cylinder similar to the Si shell of the Ge/Si core/shell NW (Figure 5c). Figures 5 d and e compare the hole density distribution in a conventional Ge/Si core/shell

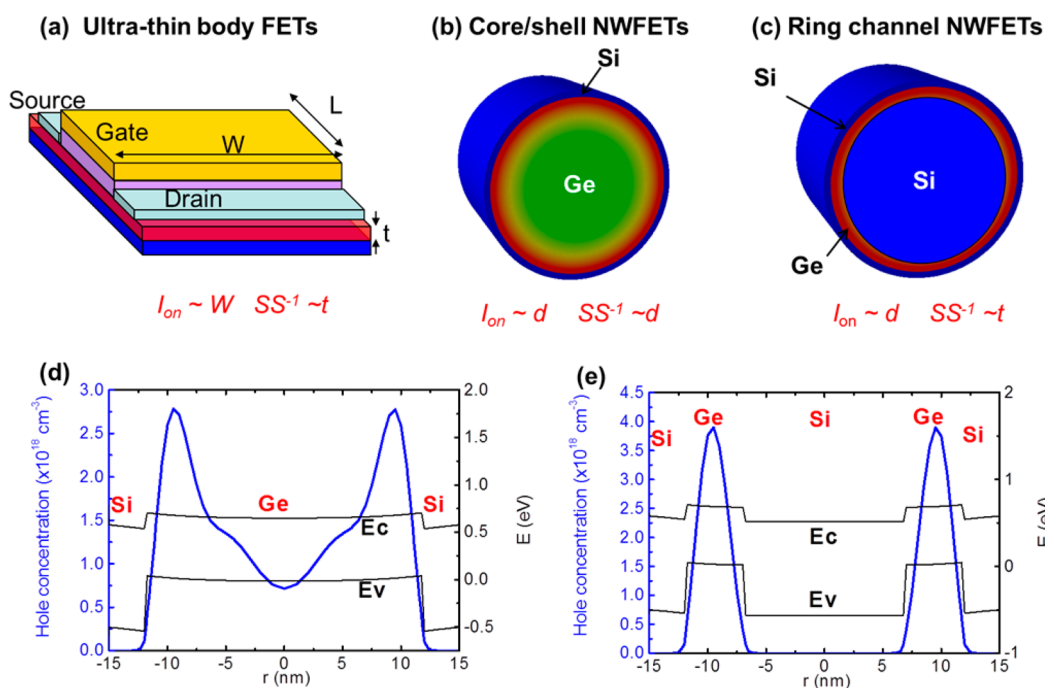


Figure 5. Schematic diagram of different FETs: (a) ultrathin body FETs, (b) core/shell NWFETs, (c) cylindrical ring channel NWFETs, and Silvaco simulation of the hole distribution in (d) a core/shell NWFET and (e) a cylindrical ring channel NWFET.

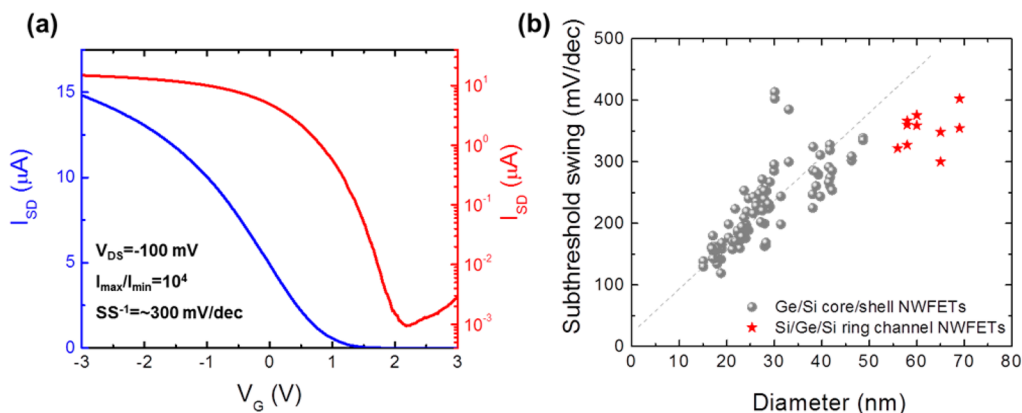


Figure 6. (a) Transfer curve $I_{SD}-V_G$ of a ring channel NWFET and (b) distribution of subthreshold swings of NWFETs in comparison to Ge/Si core/shell NWFETs (ref 20).

NW and a cylindrical ring channel Si/Ge/Si core/multishell structure. As predicted, in Ge/Si core/shell NW, holes are populated at the perimeter of the Ge core; thus, a linear dependence of transconductance with diameter was observed. However, there is a non-negligible hole distribution tailing into the core, which requires larger gate bias to deplete resulting in a larger subthreshold swing with diameter. In the Si/Ge/Si core/multishell NWs, holes are confined solely in the thin Ge ring, and the Si core is naturally depleted. It is expected that the subthreshold swing will be controlled by the thin Ge shell thickness (t), whereas the conductance remains proportional to the total diameter (d), similar to the dependency on t and w in an ultrathin body FET.^{42,43} This is analogous to an ultrathin body FET rolled into a ring (with width $w = \pi d$), with the added benefits of minimal lateral dimension and no exposed sidewalls of the conducting channel. Similar to the ultrathin body FET, the novel cylindrical ring NWFET concept requires both high quality Ge shell for high mobility electronic transport and ultrathin shell to facilitate fast ON–OFF switching with

higher transconductance, lower OFF current, and steeper subthreshold swing. Advances in understanding the core/shell growth mechanisms achieved in this study address these critical requirements.

The cylindrical ring channel NWFETs were processed and measured using the same procedures for Ge/Si core/shell NWFETs.²⁰ Shown in Figure 6a is the $I_{SD}-V_G$ transfer curve of a typical ring channel NWFET with the total diameter of 65 nm, including a 10 nm Ge channel and a channel length of 450 nm. At $V_{DS} = -100$ mV, the current attains 15 μA at -3 V gate bias, and drops by 4 orders of magnitude at the off regime. The subthreshold swing of several cylindrical ring channel NWFETs, in the range of 300–400 mV/decade, are plotted together with Ge/Si core/shell NWFETs from ref 20 (Figure 6b). Although Ge/Si core/shell NWs exhibit an increasing subthreshold swing with diameter, that of the Si/Ge/Si core/multishell devices falls below the trend. However, the cylindrical ring channel subthreshold swing is not as low as expected for a 10 nm thick Ge channel length, likely due to

insufficient coupling of the Ω -shape top gate and the bottom of the Ge channel that is screened by the top Si core above it. Further optimization of the cylindrical ring channel NWFETs requires a gate-all-around geometry, which is beyond the scope of the present work. Nevertheless, the present reduction of the subthreshold swing compared to Ge/Si core/shell NWFET confirms the advantages of cylindrical channel NWFETs and motivates future studies on cylindrical quantum well gate-all-around geometries.

In summary, we present novel observations on the nucleation and growth of Ge shell on Si core NWs. Experimental evidence of facet nucleation and the transition to conformal shell epitaxy prompts a need for a refined theoretical model to explain the growth mechanisms. The ability to grow conformal Ge shells on Si opens new prospects for core/multishell and radial superlattices in the Ge/Si material system. The first prototype of the cylindrical ring channel NWFET concept demonstrates the potential for radially heterostructured Ge/Si core/multi shell NWs in advanced electronic and optoelectronic devices.

■ ASSOCIATED CONTENT

● Supporting Information

The Supporting Information is available free of charge on the ACS Publications website at DOI: 10.1021/acs.nanolett.5b02313.

Further details of experimental methods and measurements. (PDF)

■ AUTHOR INFORMATION

Corresponding Authors

* E-mail: mbnguyen@hrl.com (B.-M. N.)

*E-mail: sdayeh@ece.ucsd.edu (S. A. D.).

Present Address

(B.-M.N.) HRL Laboratories, LLC, Malibu, California 90265, United States.

Notes

The authors declare no competing financial interest.

■ ACKNOWLEDGMENTS

This work was performed, in part, at the Center for Integrated Nanotechnologies, an Office of Science User Facility operated for the U.S. Department of Energy (DOE) Office of Science. Los Alamos National Laboratory, an affirmative action equal opportunity employer, is operated by Los Alamos National Security, LLC, for the National Nuclear Security Administration of the U.S. Department of Energy under contract DE-AC52-06NA25396. The authors would like to acknowledge Dr. Jinkyong Yoo and Katherine Jungjohann from CINT for the access to their CVD and TEM systems, respectively. B.-M.N. is grateful for a Los Alamos National Lab's Director's postdoctoral fellowship and S.A.D. acknowledges support of NSF CAREER Award under ECCS-1351980 and an NSF DMR-1503595 award.

■ REFERENCES

- (1) Lauhon, L. J.; Gudiksen, M. S.; Wang, D.; Lieber, C. M. Epitaxial core-shell and core-multishell nanowire heterostructures. *Nature* **2002**, *420* (6911), 57–61.
- (2) Raychaudhuri, S.; Yu, E. T. Critical dimensions in coherently strained coaxial nanowire heterostructures. *J. Appl. Phys.* **2006**, *99* (11), 114308.
- (3) Ertekin, E.; Greaney, P. A.; Chrzan, D. C.; Sands, T. D. Equilibrium limits of coherency in strained nanowire heterostructures. *J. Appl. Phys.* **2005**, *97* (11), 114325.
- (4) Wang, H.; Upmanyu, M.; Ciobanu, C. V. Morphology of Epitaxial Core-Shell Nanowires. *Nano Lett.* **2008**, *8* (12), 4305–4311.
- (5) Goldthorpe, I. A.; Marshall, A. F.; McIntyre, P. C. Inhibiting Strain-Induced Surface Roughening: Dislocation-Free Ge/Si and Ge/SiGe Core-Shell Nanowires. *Nano Lett.* **2009**, *9* (11), 3715–3719.
- (6) Li, X.; Yang, G. Strain Self-Releasing Mechanism in Heteroepitaxy on Nanowires. *J. Phys. Chem. C* **2009**, *113* (28), 12402–12406.
- (7) Colin, J. Prismatic dislocation loops in strained core-shell nanowire heterostructures. *Phys. Rev. B: Condens. Matter Mater. Phys.* **2010**, *82* (5), 054118.
- (8) Dayeh, S. A.; Tang, W.; Boioli, F.; Kavanagh, K. L.; Zheng, H.; Wang, J.; Mack, N. H.; Swadener, G.; Huang, J. Y.; Miglio, L.; Tu, K.-N.; Picraux, S. T. Direct Measurement of Coherency Limits for Strain Relaxation in Heteroepitaxial Core/Shell Nanowires. *Nano Lett.* **2013**, *13* (5), 1869–1876.
- (9) Goldthorpe, I. A.; Marshall, A. F.; McIntyre, P. C. Synthesis and Strain Relaxation of Ge-Core/Si-Shell Nanowire Arrays. *Nano Lett.* **2008**, *8* (11), 4081–4086.
- (10) Schmidt, V.; McIntyre, P. C.; Gösele, U. Morphological instability of misfit-strained core-shell nanowires. *Phys. Rev. B: Condens. Matter Mater. Phys.* **2008**, *77* (23), 235302.
- (11) Dayeh, S. A.; Mack, N. H.; Huang, J. Y.; Picraux, S. T. Advanced core/multishell germanium/silicon nanowire heterostructures: The Au-diffusion bottleneck. *Appl. Phys. Lett.* **2011**, *99* (2), 023102.
- (12) Lu, W.; Xiang, J.; Timko, B. P.; Wu, Y.; Lieber, C. M. One-dimensional hole gas in germanium/silicon nanowire heterostructures. *Proc. Natl. Acad. Sci. U. S. A.* **2005**, *102* (29), 10046–10051.
- (13) Xiang, J.; Lu, W.; Hu, Y.; Wu, Y.; Yan, H.; Lieber, C. M. Ge/Si nanowire heterostructures as high-performance field-effect transistors. *Nature* **2006**, *441* (7092), 489–493.
- (14) Liang, G.; Xiang, J.; Kharche, N.; Klimeck, G.; Lieber, C. M.; Lundstrom, M. Performance Analysis of a Ge/Si Core/Shell Nanowire Field-Effect Transistor. *Nano Lett.* **2007**, *7* (3), 642–646.
- (15) Hao, X.-J.; Tu, T.; Cao, G.; Zhou, C.; Li, H.-O.; Guo, G.-C.; Fung, W. Y.; Ji, Z.; Guo, G.-P.; Lu, W. Strong and Tunable Spin-Orbit Coupling of One-Dimensional Holes in Ge/Si Core/Shell Nanowires. *Nano Lett.* **2010**, *10* (8), 2956–2960.
- (16) Dayeh, S. A.; Gin, A. V.; Picraux, S. T. Advanced core/multishell germanium/silicon nanowire heterostructures: Morphology and transport. *Appl. Phys. Lett.* **2011**, *98* (16), 163112–3.
- (17) Nah, J.; Dillen, D. C.; Varahramyan, K. M.; Banerjee, S. K.; Tutuc, E. Role of Confinement on Carrier Transport in Ge-Si_xGe_{1-x} Core-Shell Nanowires. *Nano Lett.* **2012**, *12* (1), 108–112.
- (18) Hu, Y.; Kuemmeth, F.; Lieber, C. M.; Marcus, C. M. Hole spin relaxation in Ge-Si core-shell nanowire qubits. *Nat. Nanotechnol.* **2011**, *7* (1), 47–50.
- (19) Moon, J.; Kim, J.-H.; Chen, Z. C. Y.; Xiang, J.; Chen, R. Gate-Modulated Thermoelectric Power Factor of Hole Gas in Ge-Si Core-Shell Nanowires. *Nano Lett.* **2013**, *13* (3), 1196–1202.
- (20) Nguyen, B.-M.; Taur, Y.; Picraux, S. T.; Dayeh, S. A. Diameter-Independent Hole Mobility in Ge/Si Core/Shell Nanowire Field Effect Transistors. *Nano Lett.* **2014**, *14* (2), 585–591.
- (21) Dillen, D. C.; Kim, K.; Liu, E.-S.; Tutuc, E. Radial modulation doping in core-shell nanowires. *Nat. Nanotechnol.* **2014**, *9* (2), 116–120.
- (22) Yan, H.; Choe, H. S.; Nam, S.; Hu, Y.; Das, S.; Klemic, J. F.; Ellenbogen, J. C.; Lieber, C. M. Programmable nanowire circuits for nanoprocessors. *Nature* **2011**, *470* (7333), 240–244.
- (23) Yao, J.; Yan, H.; Das, S.; Klemic, J. F.; Ellenbogen, J. C.; Lieber, C. M. Nanowire nanocomputer as a finite-state machine. *Proc. Natl. Acad. Sci. U. S. A.* **2014**, *111* (7), 2431–2435.
- (24) Peng, X.; Tang, F.; Logan, P. Band structure of Si/Ge core-shell nanowires along the [110] direction modulated by external uniaxial strain. *J. Phys.: Condens. Matter* **2011**, *23* (11), 115502.

- (25) Hu, M.; Giapis, K. P.; Goicochea, J. V.; Zhang, X.; Poulidakos, D. Significant Reduction of Thermal Conductivity in Si/Ge Core–Shell Nanowires. *Nano Lett.* **2011**, *11* (2), 618–623.
- (26) Yang, L.; Musin, R. N.; Wang, X.-Q.; Chou, M. Y. Quantum confinement effect in Si/Ge core-shell nanowires: First-principles calculations. *Phys. Rev. B: Condens. Matter Mater. Phys.* **2008**, *77* (19), 195325.
- (27) Peng, X.; Logan, P. Electronic properties of strained Si/Ge core-shell nanowires. *Appl. Phys. Lett.* **2010**, *96* (14), 143119.
- (28) Liu, N.; Li, Y.-R.; Lu, N.; Yao, Y.-X.; Fang, X.-W.; Wang, C.-Z.; Ho, K.-M. Charge localization in [1 1 2] Si/Ge and Ge/Si core–shell nanowires. *J. Phys. D: Appl. Phys.* **2010**, *43* (27), 275404.
- (29) Liu, N.; Lu, N.; Yao, Y.-X.; Zhang, G.-P.; Wang, C.-Z.; Ho, K.-M. Cross-sectional aspect ratio modulated electronic properties in Si/Ge core/shell nanowires. *J. Phys. D: Appl. Phys.* **2013**, *46* (13), 135302.
- (30) Nika, D. L.; Cocemasov, A. I.; Crismari, D. V.; Balandin, A. A. Thermal conductivity inhibition in phonon engineered core-shell cross-section modulated Si/Ge nanowires. *Appl. Phys. Lett.* **2013**, *102* (21), 213109–5.
- (31) Pan, L.; Lew, K.-K.; Redwing, J. M.; Dickey, E. C. Stranski–Krastanow Growth of Germanium on Silicon Nanowires. *Nano Lett.* **2005**, *5* (6), 1081–1085.
- (32) Kwon, S.; Chen, Z. C. Y.; Kim, J.-H.; Xiang, J. Misfit-Guided Self-Organization of Anticorrelated Ge Quantum Dot Arrays on Si Nanowires. *Nano Lett.* **2012**, *12* (9), 4757–4762.
- (33) Ben-Ishai, M.; Patolsky, F. A Route to High-Quality Crystalline Coaxial Core/Multishell Ge@Si(GeSi)_n and Si@(GeSi)_n Nanowire Heterostructures. *Adv. Mater.* **2010**, *22* (8), 902–906.
- (34) Chang, H.-K.; Lee, S.-C. The growth and radial analysis of Si/Ge core-shell nanowires. *Appl. Phys. Lett.* **2010**, *97* (25), 251912.
- (35) Fukata, N.; Mitome, M.; Sekiguchi, T.; Bando, Y.; Kirkham, M.; Hong, J.-I.; Wang, Z. L.; Snyder, R. L. Characterization of Impurity Doping and Stress in Si/Ge and Ge/Si Core–Shell Nanowires. *ACS Nano* **2012**, *6* (10), 8887–8895.
- (36) Kempa, T. J.; Kim, S.-K.; Day, R. W.; Park, H.-G.; Nocera, D. G.; Lieber, C. M. Facet-Selective Growth on Nanowires Yields Multi-Component Nanostructures and Photonic Devices. *J. Am. Chem. Soc.* **2013**, *135* (49), 18354–18357.
- (37) Guo, J.-Y.; Zhang, Y.-W.; Shenoy, V. B. Morphological Evolution and Ordered Quantum Structure Formation in Hetero-epitaxial Core–Shell Nanowires. *ACS Nano* **2010**, *4* (8), 4455–4462.
- (38) Mankin, M. N.; Day, R. W.; Gao, R.; No, Y.-S.; Kim, S.-K.; McClelland, A. A.; Bell, D. C.; Park, H.-G.; Lieber, C. M. Facet-Selective Epitaxy of Compound Semiconductors on Faceted Silicon Nanowires. *Nano Lett.* **2015**, *15* (7), 4776–4782.
- (39) Day, R. W.; Mankin, M. N.; Gao, R.; No, Y.-S.; Kim, S.-K.; Bell, D. C.; Park, H.-G.; Lieber, C. M. Plateau–Rayleigh crystal growth of periodic shells on one-dimensional substrates. *Nat. Nanotechnol.* **2015**, *10* (4), 345–352.
- (40) Xie, Y. H.; Gilmer, G. H.; Roland, C.; Silverman, P. J.; Buratto, S. K.; Cheng, J. Y.; Fitzgerald, E. A.; Kortan, A. R.; Schuppler, S.; Marcus, M. A.; Citrin, P. H. Semiconductor Surface Roughness: Dependence on Sign and Magnitude of Bulk Strain. *Phys. Rev. Lett.* **1994**, *73* (22), 3006–3009.
- (41) Eaglesham, D. J.; White, A. E.; Feldman, L. C.; Moriya, N.; Jacobson, D. C. Equilibrium shape of Si. *Phys. Rev. Lett.* **1993**, *70* (11), 1643–1646.
- (42) Knoch, J.; Zhang, M.; Appenzeller, J.; Mantl, S. Physics of ultrathin-body silicon-on-insulator Schottky-barrier field-effect transistors. *Appl. Phys. A: Mater. Sci. Process.* **2007**, *87* (3), 351–357.
- (43) Colinge, J. Subthreshold slope of thin-film SOI MOSFET's. *IEEE Electron Device Lett.* **1986**, *7* (4), 244–246.